


## Research Article

# Study on the Influence of Initiation Model on the Forming Characteristics of MEFP Warhead

Guangsong Ma,<sup>1,2</sup> Guanglin He ,<sup>1</sup> Zenghui Qiao,<sup>3</sup> and Yulong Zhang<sup>4</sup>

<sup>1</sup>Science and Technology on Electromechanical Dynamic Control Laboratory, Beijing Institute of Technology, Beijing 10081, China

<sup>2</sup>Xi'an Institute of Electromechanical Information Technology, Xi'an 710065, China

<sup>3</sup>PLA Strategic Support Force, Beijing 10081, China

<sup>4</sup>Beijing Electro-Mechanical Engineering Institute, Beijing 100074, China

Correspondence should be addressed to Guanglin He; heguanglin@bit.edu.cn

Received 15 May 2021; Accepted 30 November 2021; Published 13 December 2021

Academic Editor: Azwan I. Azmi

Copyright © 2021 Guangsong Ma et al. This is an open access article distributed under the Creative Commons Attribution License, which permits unrestricted use, distribution, and reproduction in any medium, provided the original work is properly cited.

To study the influence of different initiation modes on the forming characteristics of the MEFP warhead, numerical simulations were carried out on three types of initiation modes. The numerical simulation results showed that the number of EFPs was the least by double-column multipoint synchronous initiation, the number of EFPs was the largest by the central single-point (multipoint) initiation, and single-column single-point (multipoint synchronous) detonation forms the number of EFPs between central single-point (multipoint synchronous) detonation and double-column multipoint synchronous detonation. For the MEFP warhead of a small-caliber grenade, whether it is center detonation or eccentric detonation, the EFP velocity of multipoint detonation is higher than that of the single-point detonation, the velocity of double-column multipoint eccentric synchronous detonation is 2%–9% higher than that of the single-column single-point (multipoint eccentric synchronous) detonation, the velocity of double-column multipoint eccentric synchronous detonation is 10%–17% higher than that of the central single-point (multipoint synchronous) detonation, and the velocity of single-column single-point (multipoint eccentric synchronous) detonation is 5%–17% higher than that of the central single-point (multipoint synchronous) detonation. Research results show that although the number of EFPs is reduced during eccentric single-point (multipoint simultaneous) detonation of MEFP warheads, a higher velocity can be obtained.

## 1. Introduction

As a kind of shaped charge projectile, explosively formed projectile (EFP) began to appear in the 1970s. In order to improve the hit rate and damage probability of the projectile, the multiple explosively formed projectile (MEFP) began to appear in the 1980s [1]. MEFP is a highly effective damage warhead developed on the basis of a single EFP warhead [2]. The emergence of EFP warhead technology is to deal with armored targets. The MEFP warhead technology has become one of the effective means of destroying armed personnel with the increase in the protection capabilities of armed personnel. The main factors affecting the forming characteristics of EFP include the shape of liner, liner material, liner thickness, charge length diameter ratio, and initiation model [3]. The current research on the forming characteristics of MEFP warheads

mainly focuses on two aspects. First, the axial MEFP warhead, that is, the liner, is arranged along the charge axis [4–10]; second, the circumferential MEFP warhead, that is, the liner, is arranged along the circumference of the charge [11–16]. In literature [4–15], the research on MEFP mainly focused on the material of the liner, the parameters of the liner, the parameters of the charge, and so on. In the study of initiation mode on the forming characteristics of EFP [17–21], the main focus is on the influence of single EFP forming characteristics. In the study of initiation mode on the forming characteristics of MEFP warheads, literature [7] used LS-DYNA simulation software to conduct numerical simulation studies on three initiation modes, namely, single-point initiation, ring initiation, and plane initiation; the research results show the use of plane initiation. In this way, the effective utilization rate of explosives is the highest, and the aerodynamic performance of the

projectile and the penetration effect on the target are the best. In [16], the damage effectiveness of circumferential MEFP warhead with eccentric initiation was studied by combining experiment and numerical simulation; static detonation tests were carried out for center initiation and eccentric initiation, respectively. It was found that the eccentric initiation model can effectively improve the average velocity, distribution density, and penetration ability of EFP damage elements. Through the analysis of [4–21], it can be seen that there are more researches on axial MEFP warheads by researchers at present and relatively few researches on circumferential MEFP. There are more researches on the influence of the detonation model on the forming characteristics of a single EFP; there are few studies on the influence of MEFP forming characteristics. Only [7] and [16] study the influence of detonation methods on the forming characteristics of MEFP warheads. Among them, [7] studies the effects of the detonation model on the forming characteristics of axial MEFP warheads. Literature [16] studies the influence of the initiation model on the forming characteristics of the circumferential MEFP warhead. The combination of multipoint initiation technology and MEFP warhead can not only improve the forming velocity of local EFP but also realize the directional damage function of MEFP warhead.

In order to study the influence of multipoint initiation on the forming characteristics of circumferential MEFP warhead of small-caliber grenade, a total of 12 initiation modes in three categories were designed. The first category is central initiation, including single-point central initiation, two-point central synchronous initiation in the middle, two-point central synchronous initiation near the charge end face, and four-point central synchronous initiation. The second category is single-column eccentric initiation, including single-point eccentric initiation, two-point eccentric synchronous detonation in the middle, two-point eccentric synchronous detonation near the two end faces of the charge, and four-point eccentric synchronous detonation. The third type is double-column eccentric initiation, including two-point eccentric synchronous initiation, central four-point eccentric synchronous initiation, four-point eccentric synchronous initiation near the two end faces of the charge, and eight-point eccentric synchronous initiation. Using ANSYS/ICEM, HyperMesh, and LS-DYNA cosimulation method, the designed MEFP warhead was simulated according to 12 detonation methods, and the numerical simulations were compared and analyzed.

## 2. Structural Design

**2.1. MEFP Warhead Structure Design.** The MEFP warhead charge diameter of the small-caliber grenade designed by this research institute is 32 mm; the charge height is 52 mm, the liner diameter is 9 mm, the inner wall curvature radius of liner is 12 mm, the inner wall curvature radius of the liner is 9 mm, the thickness of the center of liner is 1.15 mm, and the thickness of the shell is 1.5 mm. There are 12 liners in each row along the radial direction of the charge and four in each column along the charge circumferential direction. There are 48 liners in the entire MEFP warhead structure. The MEFP warhead structure is shown in Figure 1.

In Figure 1, for the convenience of follow-up research, one column of the MEFP warhead is marked as 1#EFP, 2#EFP, 3#EFP, and 4#EFP.

**2.2. Initiation Model Design of MEFP Warhead.** In order to study the influence of the initiation model on the forming characteristics of MEFP warheads, the following initiation modes were designed: center initiation model and eccentric initiation mode. Among them, eccentric initiation mode includes single-column eccentric initiation and double-column eccentric initiation.

The central detonation mode includes single-point detonation, two-point synchronous detonation, and four-point synchronous detonation. The structure diagram of the designed detonation point is shown in Figure 2.

In Figure 2, (a) represents a single-point detonation, which is represented by center initiation mode 1, (b) represents central two-point center synchronous initiation, which is represented by center initiation mode 2, and (c) represents a two-point synchronous detonation near the end surface, which is represented by center initiation mode 3, and (d) represents four-point synchronous initiation, which is represented by center initiation mode 4.

Single-column eccentric initiation includes single-point eccentric initiation, two-point eccentric synchronous initiation, and four-point eccentric synchronous initiation. Two-point eccentric synchronous initiation includes two-point eccentric synchronous initiation in the middle and two-point eccentric synchronous initiation near the end surface. The structure diagram of the designed initiation mode is shown in Figure 3.

In Figure 3, single-column mode 1 represents a single-column single-point eccentric initiation, as shown in Figure 3(a). Single-column mode 2 represents single-column two-point eccentric synchronous initiation in the middle of charge, as shown in Figure 3(b). Single-column mode 3 represents a single-column two-point eccentric synchronous detonations near the end face of charge, as shown in Figure 3(c). Single-column mode 4 represents a single-column four-point eccentric synchronous detonation, as shown in Figure 3(d).

Double-column eccentric initiation includes two-point eccentric synchronous initiation, four-point eccentric synchronous initiation, and eight-point eccentric synchronous initiation. Among them, four-point eccentric synchronous initiation includes four points in the middle of charge (two columns and two points) and four-point eccentric synchronous initiation near the end of charge (two columns and two points). The structure diagram of the designed initiation mode is shown in Figure 3. The angle between the initiation points of the two rows is 45°.

In the central initiation structure diagram shown in Figure 4, double-column mode 1 indicates double-column two-point eccentric synchronous initiation, as shown in Figure 4(a); double-column mode 2 refers to double-column four-point eccentric synchronous initiation in the middle of charge, as shown in Figure 4(b); double-column mode 3 refers to double-column four-point eccentric synchronous

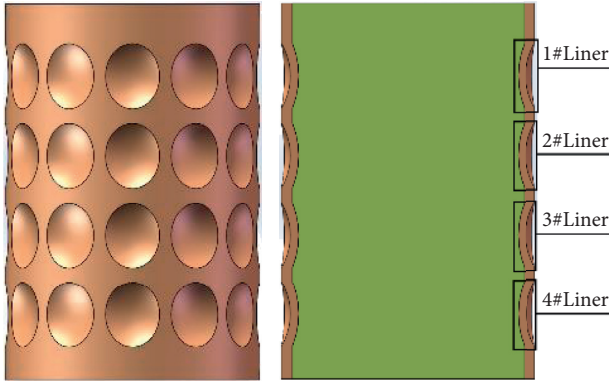


FIGURE 1: MEFP warhead structure.

initiation near the end of charge, as shown in Figure 4(c); double-column mode 4 refers to double-column eight-point eccentric synchronous initiation, as shown in Figure 4(d).

### 3. Numerical Calculation Model

**3.1. Finite Element Model.** In this study, the joint simulation method combines the advantages of ANSYS/ICEM, HyperMesh, and LS-DYNA. First, ANSYS/ICEM is used to divide the designed MEFP warhead structure into a structured mesh, and then the structured mesh is transformed into unstructured meshes and export mesh files. HyperMesh will continue the preprocessing of finite element analysis required by LS-DYNA, and finally, LS-DYNA will perform numerical calculation and postprocessing. For the central detonation, because the MEFP warhead designed by this research is a centrally symmetric structure, in order to reduce the calculation amount, a quarter finite element model of the MEFP warhead is established, the finite element model is shown in Figure 5(a). For eccentric initiation, two eccentric initiation modes are designed, namely, single-column eccentric initiation and double-column eccentric initiation. In order to better simulate the detonation wave superimposition effect of single-column eccentric initiation, the established half of the MEFP warhead model is shown in Figure 5(b); in order to better simulate the detonation wave superposition effect of double-column eccentric initiation, the complete finite element model established is shown in Figure 5(c).

**3.2. Material Model.** The material model is the same as that in Section 3.2 in [22].

## 4. Numerical Calculation Results

### 4.1. Numerical Simulation Results of the Center Detonation of the MEFP Warhead

**4.1.1. Forming Results.** Figure 6 shows the molding result when the MEFP warhead is detonated in the center.

Figure 6(a) shows the forming result of MEFP warhead with single-point initiation, and the setting of initiation point is shown in Figure 2(a); in the case of single-point center initiation, the position of detonation wave front

arriving at the liner is different, which results in a certain divergence angle of EFPs except 1#EFP. Figure 6(b) shows the forming result of two-point center synchronous initiation in the middle of charge, the initiation point is set as shown in Figure 2(b), and the difference in the positions of the explosion wave front reaching the 1#liner and 4# liner causes 1#EFP and 4#EFP to have a certain dispersion angle. The detonation wave is superimposed in the middle of the two initiation points, and the superimposed detonation wave front acts on the center of the 2#liner and 3#liner, resulting in horizontal dispersion of 2#EFP and 3#EFP along the radial direction of the charge. Figure 6(c) shows two-point center synchronous initiation near the end face of charge, and the initiation point is set as shown in Figure 2(c). During two-point center synchronous initiation near the end face of charge, the detonation wave front acts on the center of the 1#liner and the 4#liner, respectively, and the 1#EFP and 4#EFP disperse horizontally along the radial direction of the charge. As the charge detonation progresses, the detonation front first acts on the side of the 2#liner and 3#liner; when the two detonation wave fronts are superimposed, the detonation wave pressure acts on the other side of 2#liner and 3#liner, causing 2#EFP and 3#EFP to disperse horizontally along the radial direction of the charge. Figure 6(d) shows four-point center synchronous initiation, and the setting of initiation points is shown in Figure 2(d). During the four-point center synchronous initiation, the detonation wave fronts generated by the four detonation points will act on the center of 1#liner, 2# liner, 3#liner, and 4# liner, respectively, after being superimposed, resulting in horizontal dispersion of 1#EFP, 2#EFP, 3#EFP, and 4#EFP along the radial direction of the charge.

**4.1.2. Forming Velocity.** The velocity contrast curves of four different initiation modes are shown in Figure 7.

In Figure 7,  $v_{1i}$  ( $i = 1, 2, 3, 4$ ) is used to represent the forming velocity of EFP in central initiation mode 1 (e.g.,  $v_{11}$  is the velocity of 1#EFP).  $v_{2i}$  ( $i = 1, 2, 3, 4$ ) is used to represent the forming velocity of EFP in central initiation mode 2 (e.g.,  $v_{21}$  is the velocity of 1#EFP).  $v_{3i}$  ( $i = 1, 2, 3, 4$ ) is used to represent the forming velocity of EFP in central initiation mode 3 (e.g.,  $v_{31}$  is the velocity of 1#EFP).  $v_{4i}$  ( $i = 1, 2, 3, 4$ ) is used to represent the forming velocity of EFP in central initiation mode 4 (e.g.,  $v_{41}$  is the velocity of 1#EFP). Figure 7(a) shows the comparison curve of forming velocity of 1#EFP in four initiation modes; Figure 7(b) shows the comparison curve of forming velocity of 2#EFP in four initiation modes; Figure 7(c) shows the comparison curve of forming velocity of 3#EFP in four initiation modes; Figure 7(d) shows the forming velocity comparison curve of 4#EFP in the four initiation modes. As can be seen from Figure 7,  $v_{11} = 2036$  m/s,  $v_{12} = 2051$  m/s,  $v_{13} = 2096$  m/s, and  $v_{14} = 2142$  m/s;  $v_{21} = 2008$  m/s,  $v_{22} = 2249$  m/s,  $v_{23} = 2247$  m/s, and  $v_{24} = 1983$  m/s;  $v_{31} = 2117$  m/s,  $v_{32} = 2429$  m/s,  $v_{33} = 2389$  m/s, and  $v_{34} = 2075$  m/s;  $v_{41} = 2170$  m/s,  $v_{42} = 2375$  m/s,  $v_{43} = 2376$  m/s, and  $v_{44} = 2124$  m/s. In Figure 7(a), the velocity of 1#EFP in the four initiation

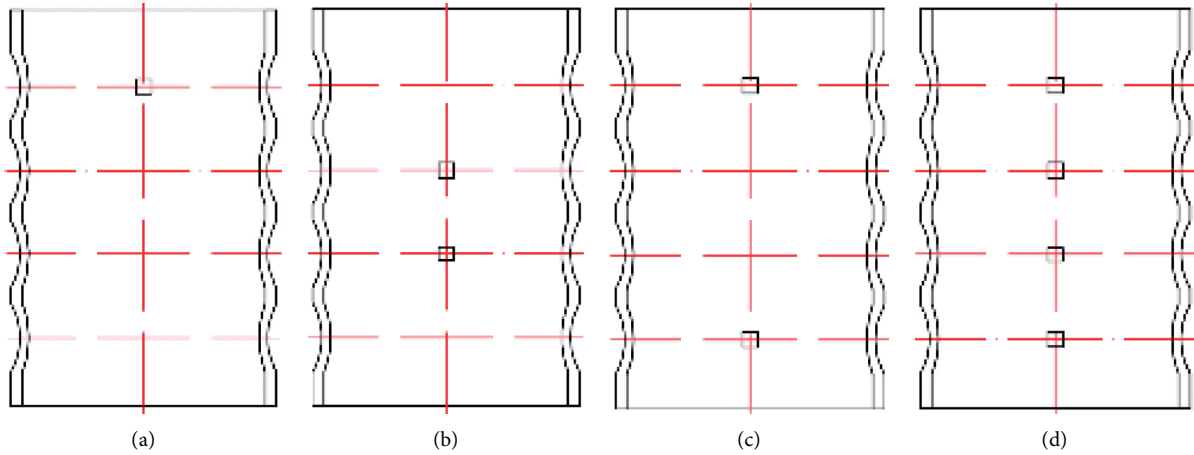


FIGURE 2: Schematic diagram of the central detonation point structure.

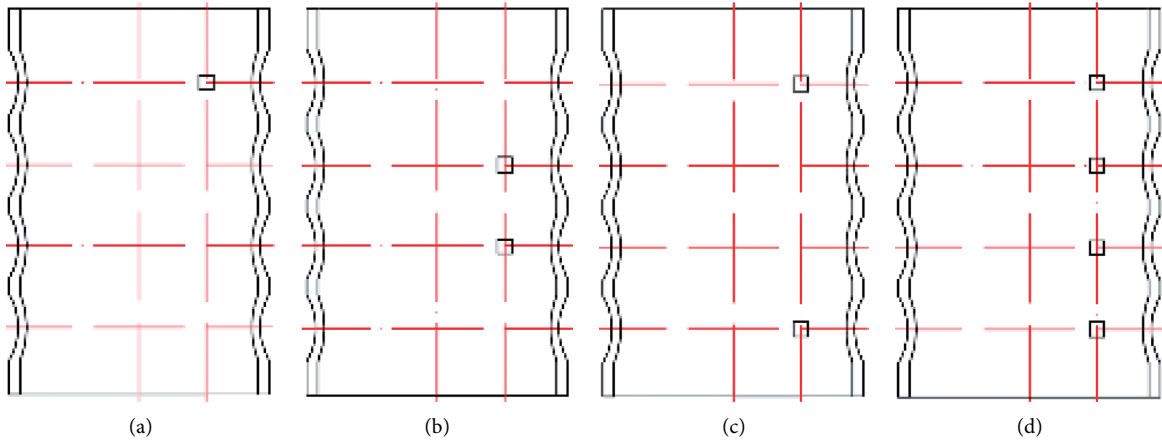


FIGURE 3: Structure diagram of single-column eccentric initiation mode.

modes is  $v_{41} > v_{31} > v_{11} > v_{21}$ . In Figure 7(b), the velocity of 2#EFP in the four initiation modes is  $v_{32} > v_{42} > v_{22} > v_{12}$ . In Figure 7(c), the velocity of 3#EFP in the four initiation modes is  $v_{33} > v_{43} > v_{23} > v_{13}$ . In Figure 7(d), the velocity of 4#EFP in the four initiation modes is  $v_{14} > v_{44} > v_{34} > v_{24}$ . Based on the above analysis, it can be seen that when the small-caliber MEFP warhead adopts a four-point center synchronous initiation or a two-point center close to the end face of charge, the EFPs can obtain a greater velocity. When the small-caliber MEFP warhead uses a single-point center initiation or a two-point center synchronous initiation in the middle of the charge, the EFP velocity is lower.

#### 4.2. Numerical Simulation Results of the Single-Column Eccentric Initiation of the MEFP Warhead

**4.2.1. Forming Results.** The forming results of single-column single-point (multipoints) eccentric synchronous initiation of small-caliber grenade MEFP warhead are shown in Figure 8, and the detonation pressure nephogram of eccentric initiation is shown in Figure 9.

In Figure 8, 1#EFP-4#EFP represents the EFPs on the side far from the initiation point, and 5#EFP-8#EFP

represents the EFPs on the side close to the initiation point. Figure 8(a) shows single-column single-point eccentric initiation, and the pressure nephogram is shown in Figure 9(a). Figure 8(b) shows single-column two-point eccentric synchronous initiation in the middle of charge, and the pressure nephogram is shown in Figure 9(b). Figure 8(c) shows single-column two-point eccentric synchronous initiation near the end face of charge, and the pressure nephogram is shown in Figure 9(c). It can be seen from Figure 8 that the liner on the side close to the initiation point does not form a better-shaped EFPs, and the liner on the side far from the initiation point can form EFPs with the head turned over. The setting of initiation position for single-column single-point initiation of MEFP warhead is shown in Figure 3(a); due to the different positions of detonation wave front arriving at the liner, there is a certain divergence angle between 2#EFP and 4#EFP. The setting of initiation position for single-column two-point eccentric synchronous initiation in the middle of charge of MEFP warhead is shown in Figure 3(b); although the initiation points are located on the horizontal line where the centers of the 2#liner and 3#liner are located respectively, due to the superposition of detonation waves, as shown in Figure 9(b), the detonation wave



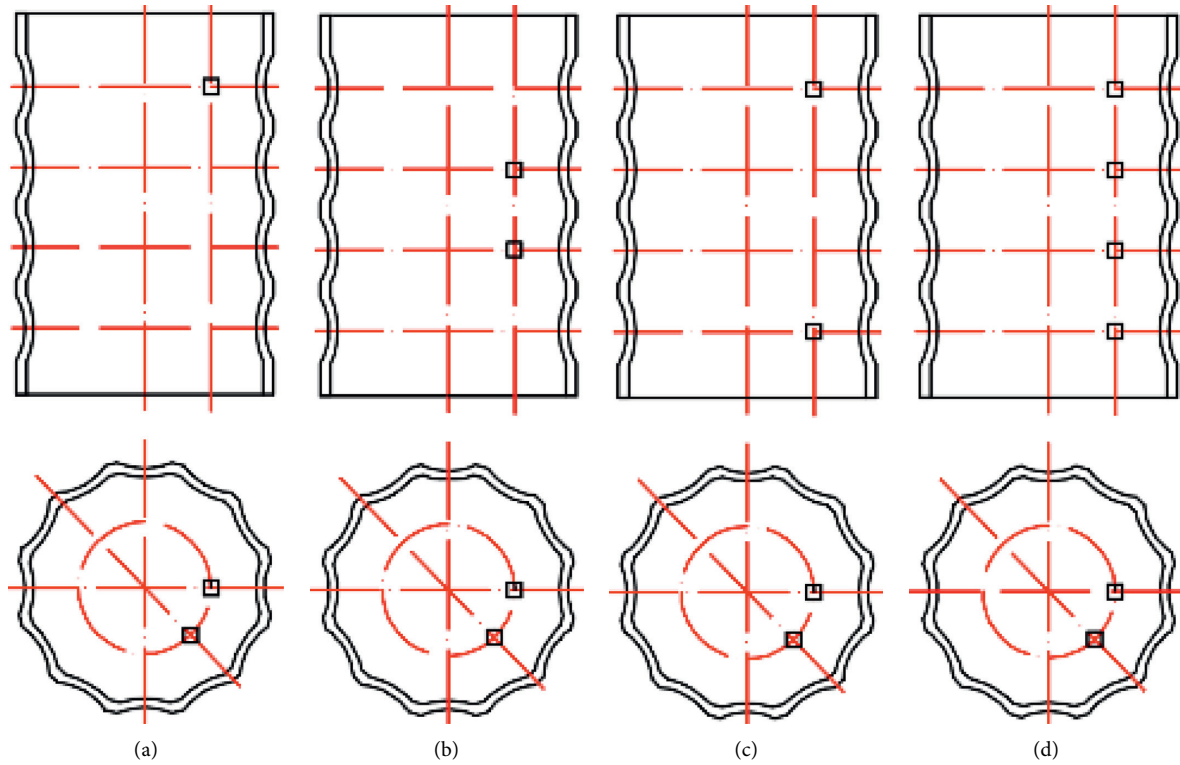


FIGURE 4: Structure diagram of double-column eccentric initiation mode.

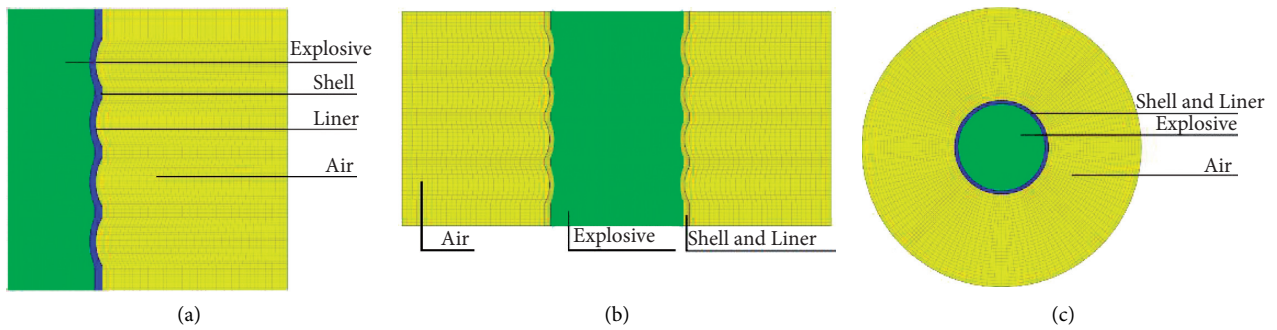


FIGURE 5: Finite element model.

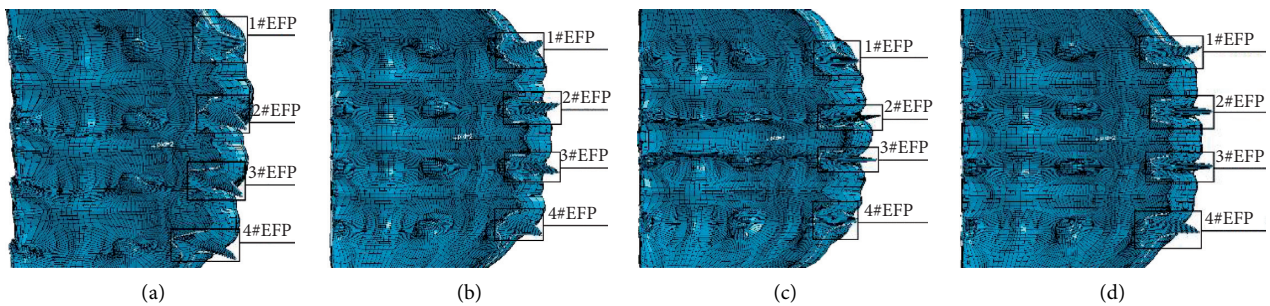


FIGURE 6: Forming results.

front is in contact near the center of the 2#liner and the 3#liner; as a result, 2#EFP and 3#EFP formed a certain divergence angle. The setting of initiation position for single-column two-point eccentric synchronous initiation near the

end face of charge of MEFP warhead is shown in Figure 3(c); in the initial stage of initiation, the detonation wave front acts on the center of the 1#EFP and 4#EFP, respectively, so that the 1#EFP and 4#EFP scatter along the radial horizontal

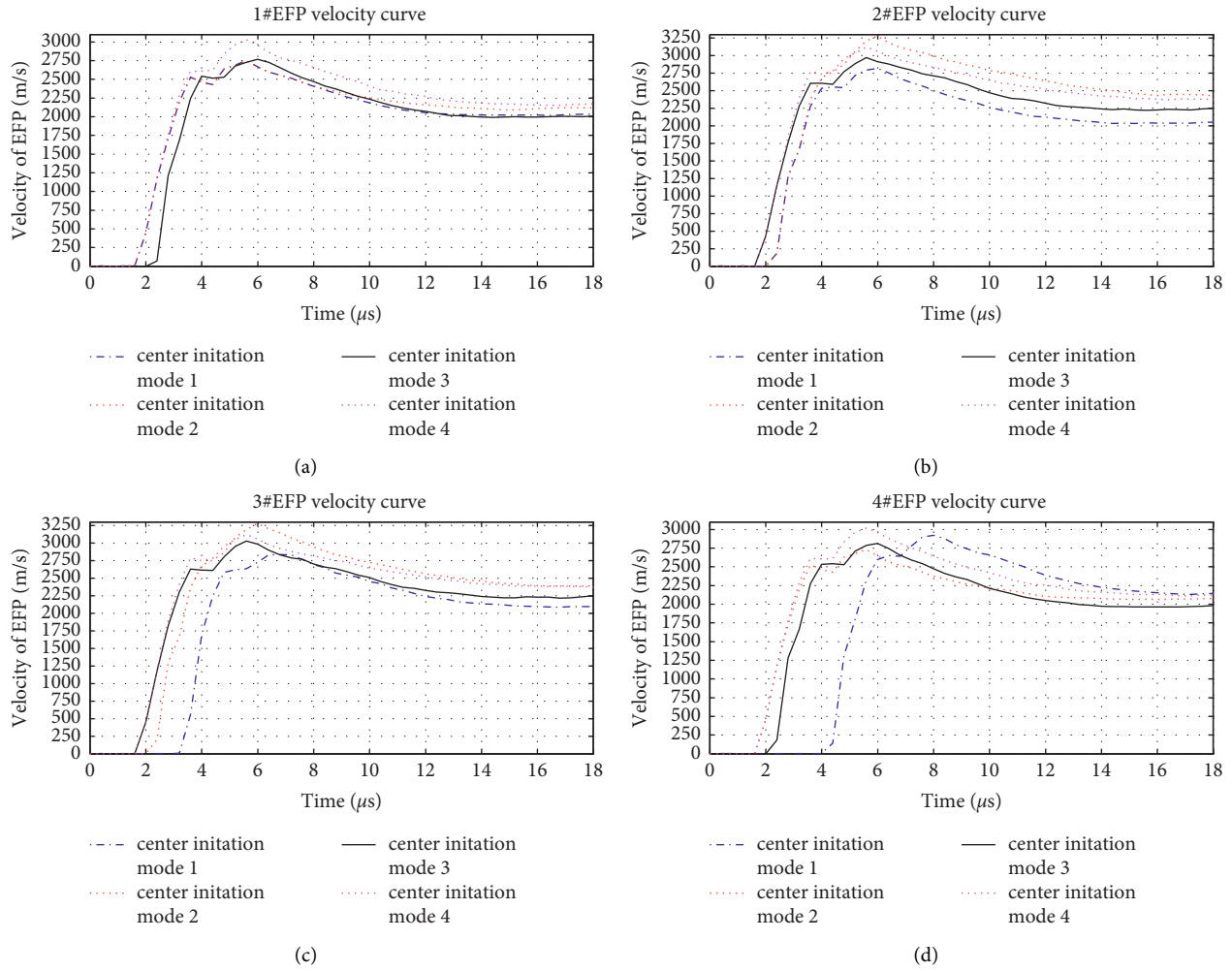


FIGURE 7: Comparison of forming velocity.

direction and the maximum pressure after detonation wave superposition is in the middle of 2#EFP and 3#EFP, as shown in Figure 9(c), resulting in 2#EFP and 3#EFP flying away along a radial direction at a certain divergence angle. As the detonation progresses, the superimposed detonation wave pressure diffuses from the middle of 2#EFP and 3#EFP to 1#EFP and 4#EFP, respectively, which results in the formation of certain dispersion angle of 1#EFP and 4#EFP along the radial direction of the charge. The setting of the initiation position for a single-column four-point eccentric synchronous initiation is shown in Figure 3(d). Due to the comprehensive action of detonation wave generated by initiation point on the horizontal line of center of 4#liner and detonation wave generated by initiation point on the horizontal line with center of 2#liner and 3#liner, this results in the fact that 3#EFP disperses horizontally along the radial direction of the charge, while the 4#EFP has a certain dispersion angle along the radial direction of the charge. Due to the comprehensive action of detonation wave generated by initiation point on the horizontal line of center of 1#liner and detonation wave generated by initiation point on the horizontal line with center of 2#liner and 3#liner, this results in the fact that 2#EFP disperses horizontally along the radial

direction of the charge, while the 1#EFP has a certain dispersion angle along the radial direction of the charge. The pressure nephogram of detonation wave of single-column four-point eccentric synchronous initiation is shown in Figure 9(d).

**4.2.2. Comparison Diagrams of Forming Velocity.** The forming velocity comparison diagram of small-caliber MEFP warhead in single-column eccentric initiation modes is shown in Figure 9.

In Figure 10,  $k_{1i}$  ( $i = 1, 2, 3, 4$ ) is used to represent the forming velocity of EFP in single-column mode 1 (e.g.,  $k_{11}$  is the velocity of 1#EFP).  $k_{2i}$  ( $i = 1, 2, 3, 4$ ) is used to represent the forming velocity of EFP in single-column mode 2 (e.g.,  $k_{21}$  is the velocity of 1#EFP).  $k_{3i}$  ( $i = 1, 2, 3, 4$ ) is used to represent the forming velocity of EFP in single-column mode 3 (e.g.,  $k_{31}$  is the velocity of 1#EFP).  $k_{4i}$  ( $i = 1, 2, 3, 4$ ) is used to represent the forming velocity of EFP in single-column mode 4 (e.g.,  $k_{41}$  is the velocity of 1#EFP). Figure 10(a) shows the comparison curve of forming velocity of 1#EFP in four initiation modes; Figure 10(b) shows the comparison curve of forming velocity of 2#EFP in four

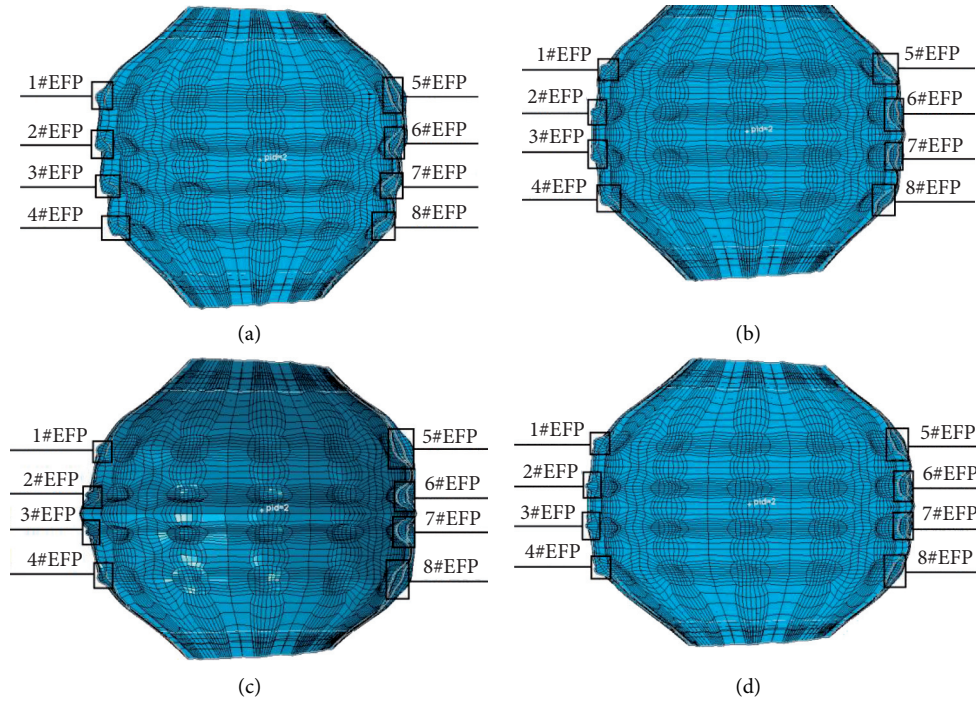


FIGURE 8: Forming results of single-column eccentric initiation.

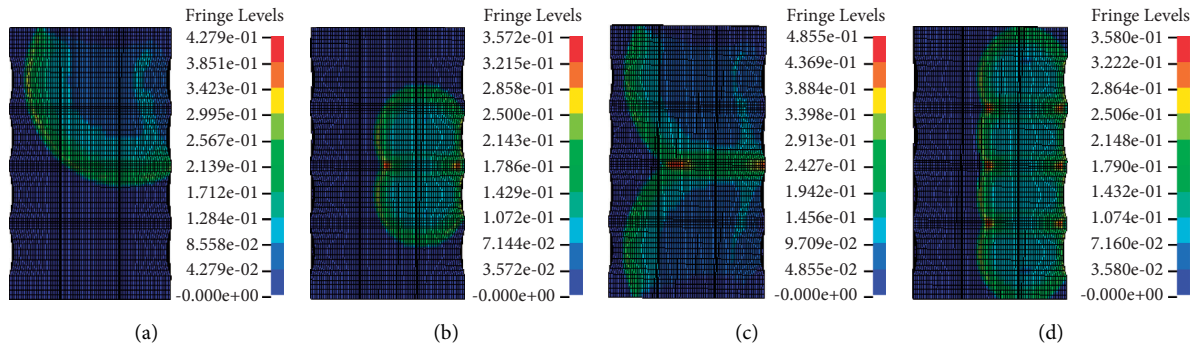


FIGURE 9: Pressure nephogram of single-column eccentric initiation.

initiation modes; Figure 10(c) shows the comparison curve of forming velocity of 3#EFP in four initiation modes; Figure 10(d) shows the forming velocity comparison curve of 4#EFP in the four initiation modes. As can be seen from Figure 10,  $k_{11} = 2192$  m/s,  $k_{12} = 2338$  m/s,  $k_{13} = 2298$  m/s, and  $k_{14} = 2251$  m/s;  $k_{21} = 2311$  m/s,  $k_{22} = 2492$  m/s,  $k_{23} = 2498$  m/s, and  $k_{24} = 2278$  m/s;  $k_{31} = 2236$  m/s,  $k_{32} = 2562$  m/s,  $k_{33} = 2578$  m/s, and  $k_{34} = 2225$  m/s;  $k_{41} = 2362$  m/s,  $k_{42} = 2606$  m/s,  $k_{43} = 2602$  m/s, and  $k_{44} = 2320$  m/s. In Figure 10(a), the velocity of 1#EFP in the four initiation modes is  $k_{41} > k_{21} > k_{31} > k_{11}$ . In Figure 10(b), the velocity of 2#EFP in the four initiation modes is  $k_{42} > k_{22} > k_{32} > k_{12}$ . In Figure 10(c), the velocity of 3#EFP in the four initiation modes is  $k_{43} > k_{33} > k_{23} > k_{13}$ . In Figure 10(d), the velocity of 4#EFP in the four initiation modes is  $k_{44} > k_{24} > k_{34} > k_{14}$ . Based on the above analysis, it can be seen that, during a single-column single-point (multipoints) eccentric synchronous initiation of MEFP warheads, the four-point

eccentric synchronous initiation has the highest velocity, and the single-column single-point eccentric synchronous initiation has the lowest velocity.

#### 4.3. Numerical Simulation Results of the Double-Column Eccentric Initiation of the MEFP Warhead

4.3.1. Forming Results. The forming result of the small-caliber grenade MEFP warhead with double-column single-point (multipoints) eccentric synchronous detonation is shown in Figure 11.

Figure 11(e) shows the top view of Figures 11(a), Figure 11(f) shows the top view of Figure 11(b), Figure 11(g) shows the top view of Figures 11(c), and Figure 11(f) shows the top view of Figure 11(d). It can be seen from Figure 11 that, during the double-column multipoints eccentric synchronously initiation the small-caliber grenade MEFP



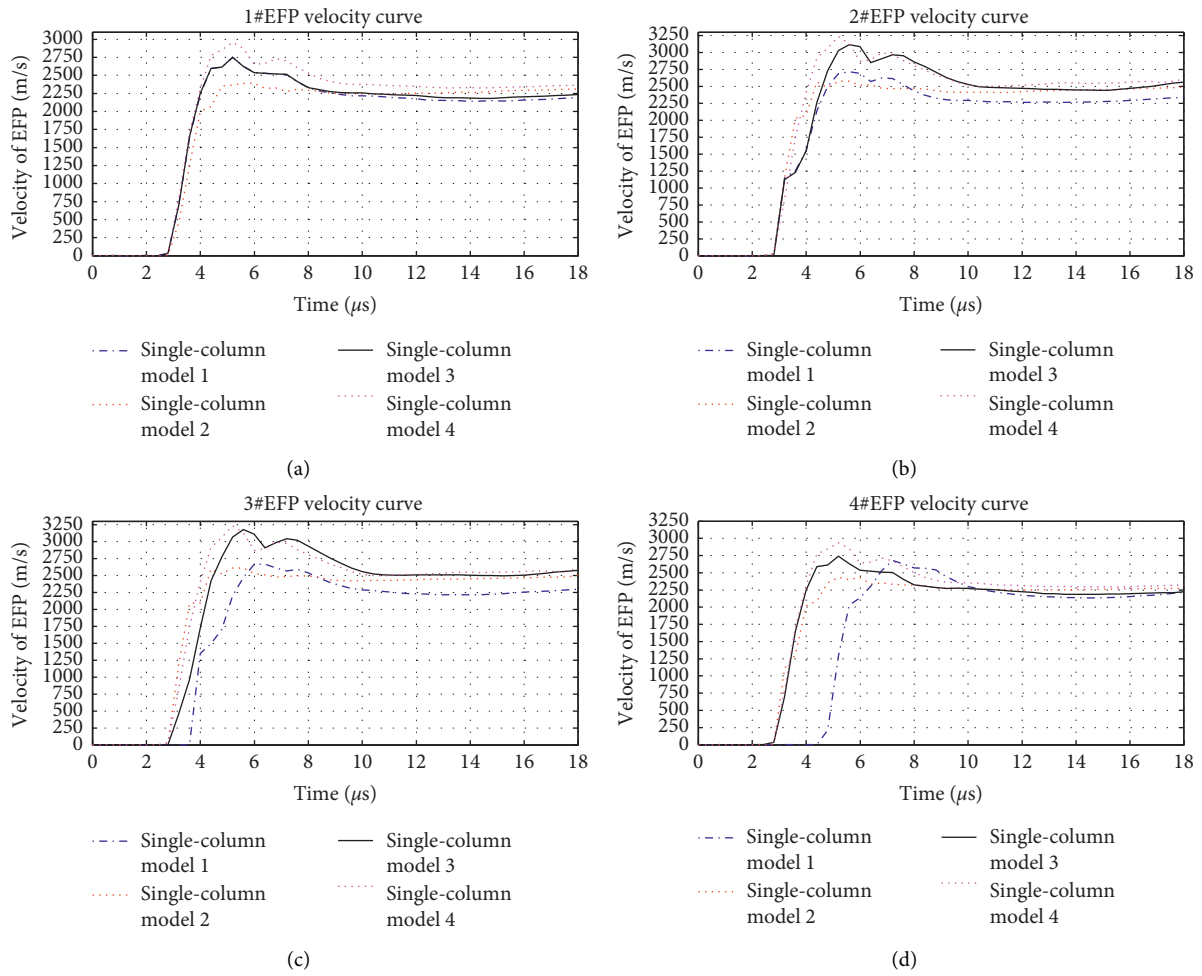


FIGURE 10: Forming velocity comparison of single-column eccentric initiation.

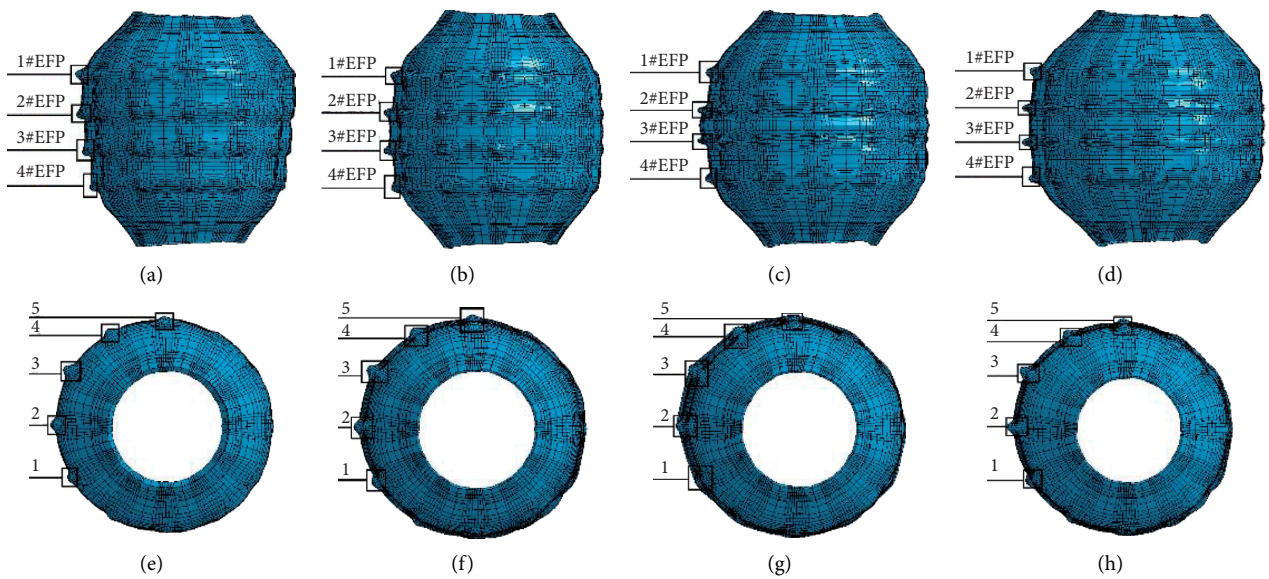


FIGURE 11: The forming result of double-column multipoints synchronous initiation.

warhead, 5 of the 12 columns designed liner can form EFP, which is marked as 1, 2, 3, 4, and 5 in Figures 11(e)–11(h)). Due to the superposition of detonation waves, the velocity of the EFP in the second or third column is the highest. By comparing the velocity of the EFPs in the second and third columns, the speed of the EFP in the third column is higher, and the EFP in the third column is marked as 1#EFP, 2#EFP, 3#EFP, and 4#EFP. It can be seen from Figure 11(a) that, except for 1#EFP, 2#EFP, 3#EFP, and 4#EFP have certain divergence angles. In Figure 11(b), since the initiation point is set at four points in the middle of charge, the maximum pressure after detonation wave superposition is located in the middle of 2#EFP and 3#EFP; therefore, the scattering directions of 1#EFP and 2#EFP deviate from the charge radial level upward, and the scattering directions of 3#EFP and 4#EFP deviate from the charge radial level downward. In Figure 11(c), since the initiation point is set near the end face of charge, the maximum pressure after detonation wave superposition is located in the middle of 2#EFP and 3#EFP; therefore, the scattering directions of 1#EFP and 2#EFP deviate from the charge radial level upward, and the scattering directions of 3#EFP and 4#EFP deviate from the charge radial level downward. In Figure 11(d), due to the interaction of the detonation wave, 2#EFP and 3#EFP are scattered along the horizontal direction of the charge, 1#EFP deviates from the charge radial level upward, and the scattering directions of 4#EFP deviate from the charge radial level downward.

**4.3.2. Forming Velocity.** The forming result of the small-caliber grenade MEFP warhead double-column multipoints eccentric synchronous initiation is shown in Figure 12.

In Figure 12,  $(m)_{1i}$  ( $i = 1, 2, 3, 4$ ) is used to represent the forming velocity of EFP in double-column mode 1 (e.g.,  $m_{11}$  is the velocity of 1#EFP).  $m_{2i}$  ( $i = 1, 2, 3, 4$ ) is used to represent the forming velocity of EFP in double-column mode 2 (e.g.,  $m_{21}$  is the velocity of 1#EFP).  $m_{3i}$  ( $i = 1, 2, 3, 4$ ) is used to represent the forming velocity of EFP in single-column mode 3 (e.g.,  $m_{31}$  is the velocity of 1#EFP).  $m_{4i}$  ( $i = 1, 2, 3, 4$ ) is used to represent the forming velocity of EFP in double-column mode 4 (e.g.,  $m_{41}$  is the velocity of 1#EFP). Figure 12(a) shows the comparison curve of forming velocity of 1#EFP in four initiation modes; Figure 12(b) shows the comparison curve of forming velocity of 2#EFP in four initiation modes; Figure 12(c) shows the comparison curve of forming velocity of 3#EFP in four initiation modes; Figure 12(d) shows the forming velocity comparison curve of 4#EFP in the four initiation modes. As can be seen from Figure 12,  $m_{11} = 2346$  m/s,  $m_{12} = 2471$  m/s,  $m_{13} = 2456$  m/s, and  $m_{14} = 2381$  m/s;  $m_{21} = 2368$  m/s,  $m_{22} = 2623$  m/s,  $m_{23} = 2608$  m/s, and  $m_{24} = 2392$  m/s;  $m_{31} = 2418$  m/s,  $m_{32} = 2789$  m/s,  $m_{33} = 2771$  m/s, and  $m_{34} = 2423$  m/s;  $m_{41} = 2487$  m/s,  $m_{42} = 2814$  m/s,  $m_{43} = 2807$  m/s, and  $m_{44} = 2506$  m/s. In Figure 12(a), the velocity of 1#EFP in the four initiation modes is  $m_{41} > m_{31} > m_{21} > m_{11}$ . In Figure 10(b), the velocity of 2#EFP in the four initiation modes is  $m_{42} > m_{32} > m_{22} > m_{12}$ . In Figure 10(c), the velocity of 3#EFP in the four initiation modes is  $m_{43} > m_{33} > m_{23} > m_{13}$ . In Figure 10(d),

the velocity of 4#EFP in the four initiation modes is  $m_{44} > m_{34} > m_{24} > m_{14}$ . Based on the above analysis, it can be seen that, during a double-column multipoints eccentric synchronous initiation of MEFP warheads, the double-column eight-point eccentric synchronous initiation has the highest velocity, and the double-column two-point eccentric initiation has the lowest velocity.

**4.4. Velocity Comparison of Different Initiation Modes.** In order to more clearly analyze the velocity difference between the three types of initiation modes, the 12 different initiation modes under the three types of initiation modes are divided into four groups. The first group is single-point central initiation, single-column single-point eccentric initiation, and double-column two-point synchronous initiation. The second group is the two-point center synchronous detonation in the middle of charge, the single-column two-point eccentric synchronous initiation in the middle of charge, and the double-column four-point eccentric synchronous initiation in the middle of charge. The third group is the two-point center synchronous initiation near the end face of charge, the single-column two-point eccentric synchronous initiation near the end face of charge, and the double-column four-point eccentric synchronous initiation near the end face of charge. The fourth group is central four-point synchronous detonation, single-column four-point eccentric synchronous initiation, and double row eight-point eccentric synchronous initiation.

**4.4.1. The Velocity Comparison of the First Group.** The velocity comparison diagrams of the first group are shown in Figure 13.

In the velocity comparison diagrams of the first group, the velocity of 1#EFP is  $m_{11} > k_{11} > v_{11}$ , which is ( $m_{11} = 2346$  m/s) > ( $k_{11} = 2192$  m/s) > ( $v_{11} = 2036$  m/s). The velocity of the double-column model 1 is 6.6% higher than that of the single-column model 1, the velocity of double-column model 2 is 13.2% higher than that center initiation model 1, and the velocity of the single-column model is 7.1% higher than the velocity of the center initiation model 1. The velocity of 2#EFP is  $m_{12} > k_{12} > v_{12}$ , which is ( $m_{12} = 2471$  m/s) > ( $k_{12} = 2338$  m/s) > ( $v_{12} = 2051$  m/s). The velocity of the double-column model 1 is 5.4% higher than that of the single-column model 1, the velocity of the double-column model 1 is 17% higher than that of the center initiation model 1, and the velocity of the single-column model 1 is 12.3% higher than the velocity of the center initiation model 1. The velocity of 3#EFP is  $m_{13} > k_{13} > v_{13}$ , which is ( $m_{13} = 2456$  m/s) > ( $k_{13} = 2298$  m/s) > ( $v_{13} = 2096$  m/s). The velocity of the double-column model 1 is 6.4% higher than that of the single-column model 1, the velocity of the double-column model 1 is 14.7% higher than that of the center initiation model 1, and the velocity of the single-column model 1 is 8.8% higher than the velocity of the center initiation model 1. The velocity of 4#EFP is  $m_{14} > k_{14} > v_{14}$ , which is ( $m_{14} = 2381$  m/s) > ( $k_{14} = 2251$  m/s) > ( $v_{14} = 2142$  m/s). The velocity of the double-column model 1 is 5.5% higher than that of the



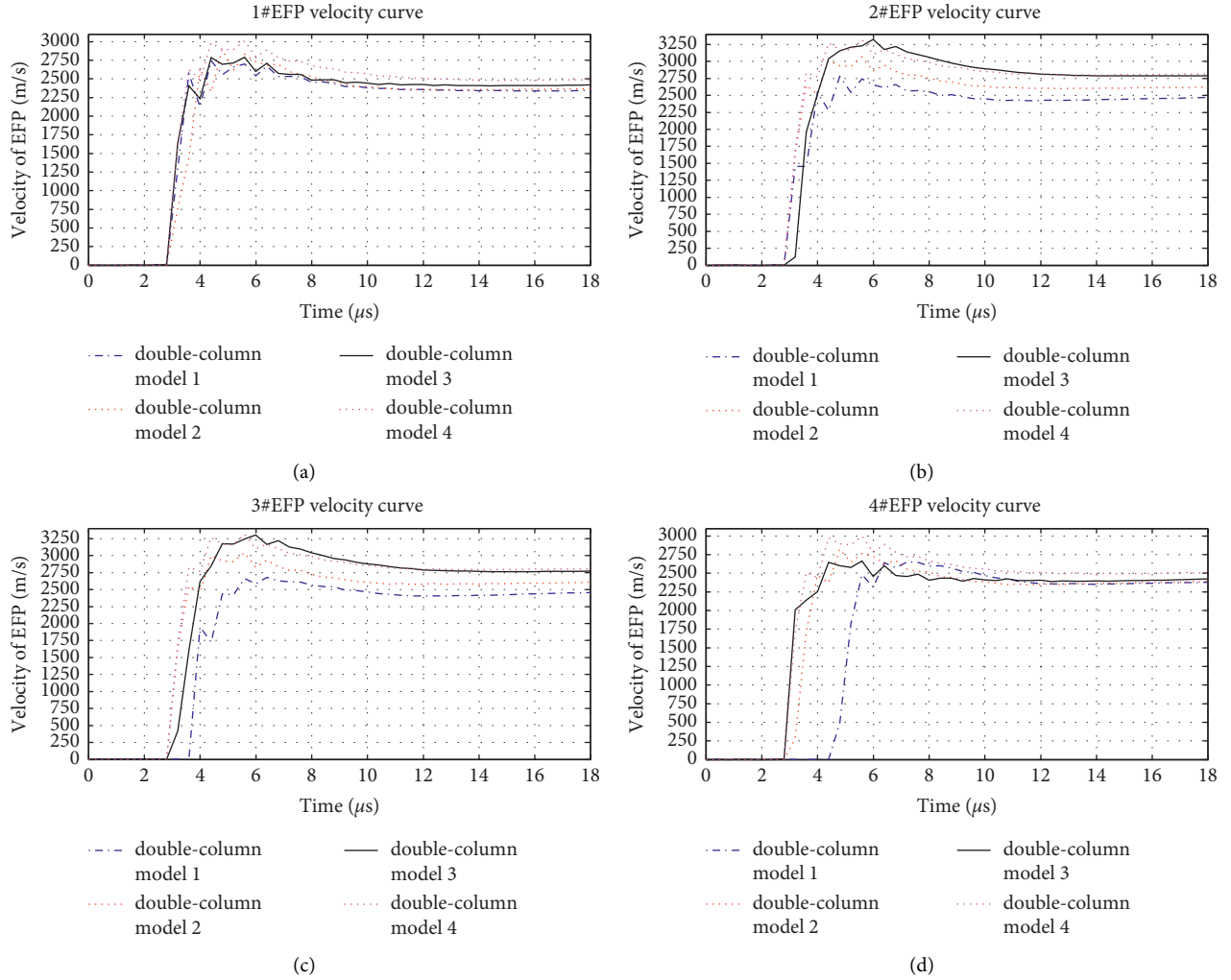


FIGURE 12: Comparison of forming velocity of double-column eccentric synchronous initiation.

single-column model 1, the velocity of the double-column model 1 is 10% higher than that of the center initiation model 1, and the velocity of the single-column model 1 is 4.8% higher than the velocity of the center initiation model 1. From the above data, it can be seen that the velocity of the double-column model 1 is 5%–7% higher than that of the single-column model 1, the velocity of the double-column model 1 is 10%–17% higher than that of the center initiation model 1, and the velocity of the single-column model 1 is 5%–13% higher than that of the center initiation model 1.

**4.4.2. The Velocity Comparison of the Second Group.** The velocity comparison diagrams of the second group are shown in Figure 14.

In the velocity comparison diagrams of the second group, the velocity of 1#EFP is  $m_{21} > k_{21} > v_{21}$ , which is  $(m_{21} = 2368 \text{ m/s}) > (k_{21} = 2311 \text{ m/s}) > (v_{21} = 2008 \text{ m/s})$ . The velocity of the double-column model 2 is 2.4% higher than that of the single-column model 2, the velocity of the double-column model 2 is 15.2% higher than that of the center initiation model 2, and the

velocity of the single-column model 2 is 13.1% higher than the velocity of the center initiation model 2. The velocity of 2#EFP is  $m_{22} > k_{22} > v_{22}$ , which is  $(m_{22} = 2623 \text{ m/s}) > (k_{22} = 2492 \text{ m/s}) > (v_{22} = 2249 \text{ m/s})$ . The velocity of the double-column model 2 is 5% higher than that of the single-column model 2, the velocity of the double-column model 2 is 14.3% higher than that of the center initiation model 2, and the velocity of the single-column model 2 is 9.8% higher than the velocity of the center initiation model 2. The velocity of 3#EFP is  $m_{23} > k_{23} > v_{23}$ , which is  $(m_{23} = 2608 \text{ m/s}) > (k_{23} = 2498 \text{ m/s}) > (v_{23} = 2247 \text{ m/s})$ . The velocity of the double-column model 2 is 4.2% higher than that of the single-column model 2, the velocity of the double-column model 2 is 13.8% higher than that of the center initiation model 2, and the velocity of the single-column model 2 is 10% higher than the velocity of the center initiation model 2. The velocity of 4#EFP is  $m_{24} > k_{24} > v_{24}$ , which is  $(m_{24} = 2392 \text{ m/s}) > (k_{24} = 2278 \text{ m/s}) > (v_{24} = 1983 \text{ m/s})$ . The velocity of the double-column model 2 is 2.1% higher than that of the single-column model 2, the velocity of the double-column model 2 is 10% higher than that of the center initiation model 2, and the velocity of the single-column model 2 is 17.1% higher than the velocity of the center

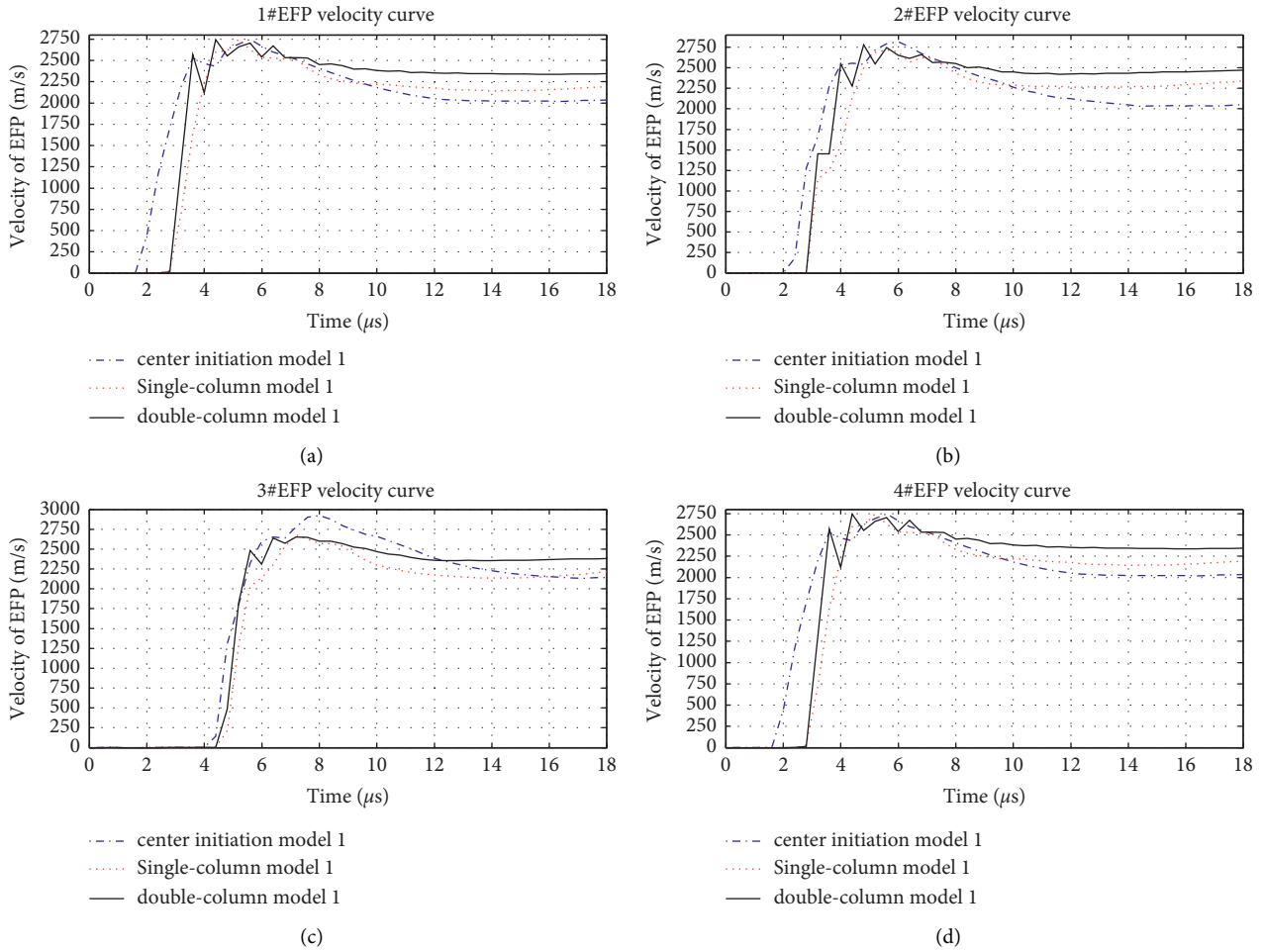


FIGURE 13: The velocity comparison of the first group.

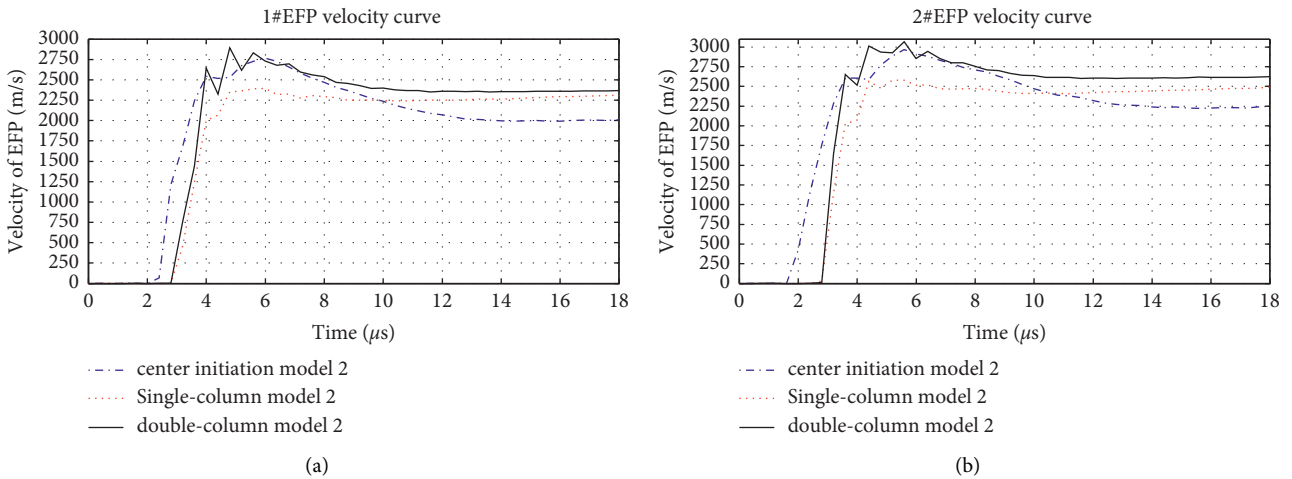


FIGURE 14: Continued.

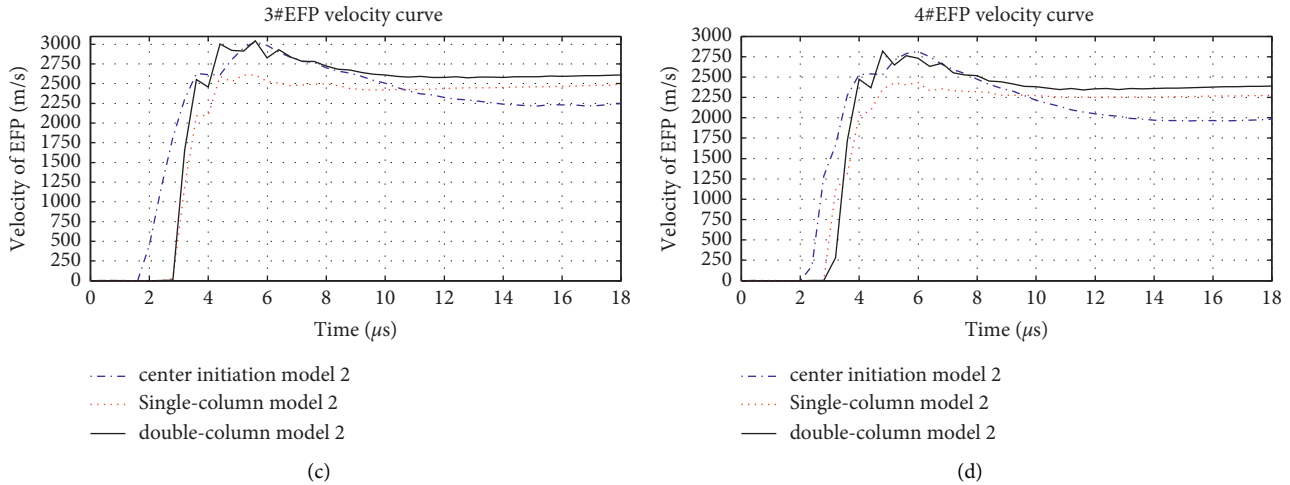


FIGURE 14: The velocity comparison of the second group.

initiation model 2. From the above data, it can be seen that the velocity of the double-column model 2 is 2%–5% higher than that of the single-column model 2, the velocity of the double-column model 2 is 10%–15% higher than that of the center initiation model 2, and the velocity of the single-column model 2 is 10%–17% higher than that of the center initiation model 2.

**4.4.3. The Velocity Comparison of the Third Group.** The velocity comparison diagrams of the third group are shown in Figure 15.

In the velocity comparison diagrams of the third group, the velocity of 1#EFP is  $m_{31} > k_{31} > v_{21}$ , which is  $(m_{31} = 2418 \text{ m/s}) > (k_{31} = 2236 \text{ m/s}) > (v_{31} = 2117 \text{ m/s})$ . The velocity of the double-column model 3 is 7.5% higher than that of the single-column model 3, the velocity of the double-column model 3 is 12.4% higher than that of the center initiation model 3, and the velocity of the single-column model 3 is 5.3% higher than the velocity of the center initiation model 3. The velocity of 2#EFP is  $m_{32} > k_{32} > v_{32}$ , which is  $(m_{32} = 2789 \text{ m/s}) > (k_{32} = 2562 \text{ m/s}) > (v_{32} = 2429 \text{ m/s})$ . The velocity of the double-column model 3 is 8.1% higher than that of the single-column model 3, the velocity of the double-column model 3 is 12.9% higher than that of the center initiation model 3, and the velocity of the single-column model 3 is 5.2% higher than the velocity of the center initiation model 3. The velocity of 3#EFP is  $m_{33} > k_{33} > v_{33}$ , which is  $(m_{33} = 2771 \text{ m/s}) > (k_{33} = 2578 \text{ m/s}) > (v_{33} = 2389 \text{ m/s})$ . The velocity of the double-column model 3 is 7% higher than that of the single-column model 3, the velocity of the double-column model 3 is 13.8% higher than that of the center initiation model 3, and the velocity of the single-column model 3 is 7.3% higher than the velocity of the center initiation model 3. The velocity of 4#EFP is  $m_{34} > k_{34} > v_{24}$ , which is  $(m_{34} = 2423 \text{ m/s}) > (k_{34} = 2225 \text{ m/s}) > (v_{34} = 2075 \text{ m/s})$ . The velocity of the double-column model 3 is 8.2% higher than that of the single-column model 3, the velocity of the double-column model 3 is 14.4% higher than that of the center initiation model 3, and the velocity of the single-column model 3 is 6.7% higher than the velocity of the center

initiation model 3. From the above data, it can be seen that the velocity of the double-column model 3 is 7%–8.5% higher than that of the single-column model 3, the velocity of the double-column model 3 is 13%–15% higher than that of the center initiation model 3, and the velocity of the single-column model 3 is 5%–7.5% higher than that of the center initiation model 3.

**4.4.4. The Velocity Comparison of the Fourth Group.** The velocity comparison diagrams of the fourth group are shown in Figure 16.

In the velocity comparison diagrams of the third group, the velocity of 1#EFP is  $m_{41} > k_{41} > v_{41}$ , which is  $(m_{41} = 2487 \text{ m/s}) > (k_{41} = 2362 \text{ m/s}) > (v_{41} = 2170 \text{ m/s})$ . The velocity of the double-column model 4 is 5% higher than that of the single-column model 4, the velocity of the double-column model 4 is 12.7% higher than that of the center initiation model 4, and the velocity of the single-column model 4 is 8.1% higher than the velocity of the center initiation model 4. The velocity of 2#EFP is  $m_{42} > k_{42} > v_{42}$ , which is  $(m_{42} = 2814 \text{ m/s}) > (k_{42} = 2606 \text{ m/s}) > (v_{42} = 2375 \text{ m/s})$ . The velocity of the double-column model 4 is 7.4% higher than that of the single-column model 4, the velocity of the double-column model 4 is 15.6% higher than that of the center initiation model 4, and the velocity of the single-column model 4 is 8.9% higher than the velocity of the center initiation model 4. The velocity of 3#EFP is  $m_{43} > k_{43} > v_{43}$ , which is  $(m_{43} = 2807 \text{ m/s}) > (k_{43} = 2602 \text{ m/s}) > (v_{43} = 2376 \text{ m/s})$ . The velocity of the double-column model 4 is 7.3% higher than that of the single-column model 4, the velocity of the double-column model 4 is 15.4% higher than that of the center initiation model 4, and the velocity of the single-column model 4 is 8.7% higher than the velocity of the center initiation model 4. The velocity of 4#EFP is  $m_{44} > k_{44} > v_{44}$ , which is  $(m_{44} = 2506 \text{ m/s}) > (k_{44} = 2320 \text{ m/s}) > (v_{44} = 2124 \text{ m/s})$ . The velocity of the double-column model 4 is 7.4% higher than that of the single-column model 4, the velocity of the double-column model 4 is 15.2% higher than that of the center initiation model 4, and the velocity of the single-

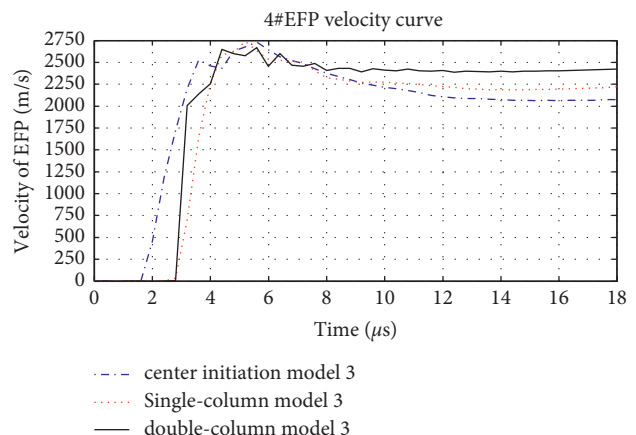
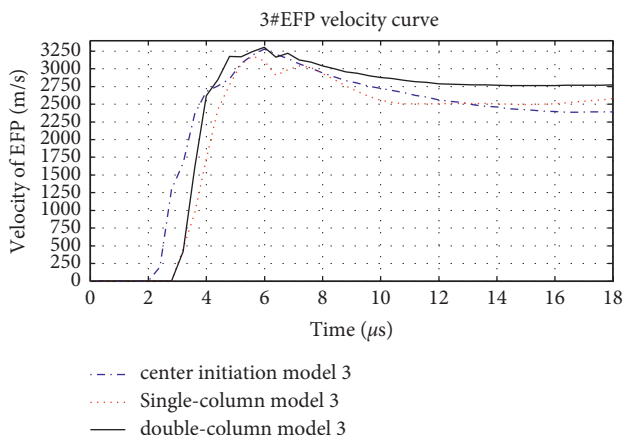
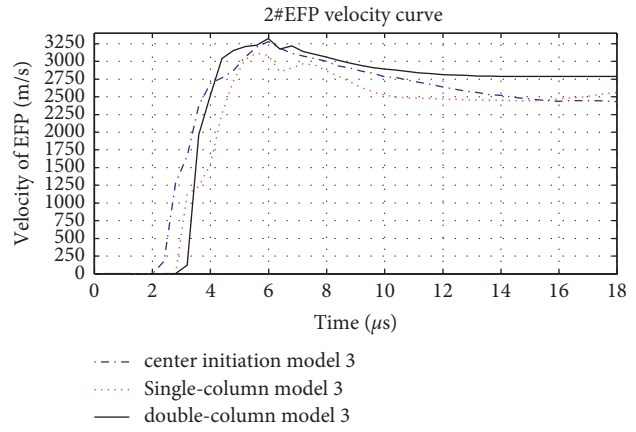
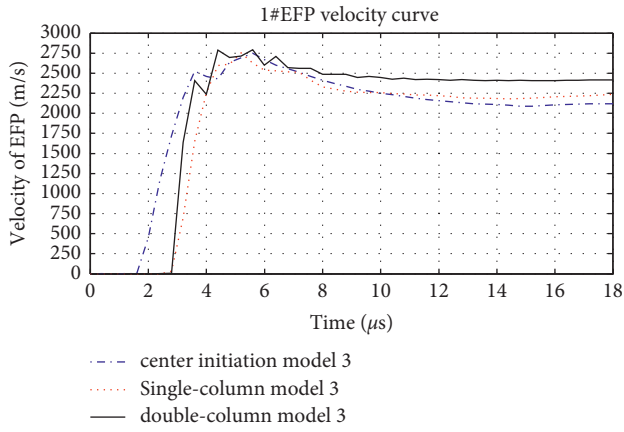


FIGURE 15: The velocity comparison of the third group.

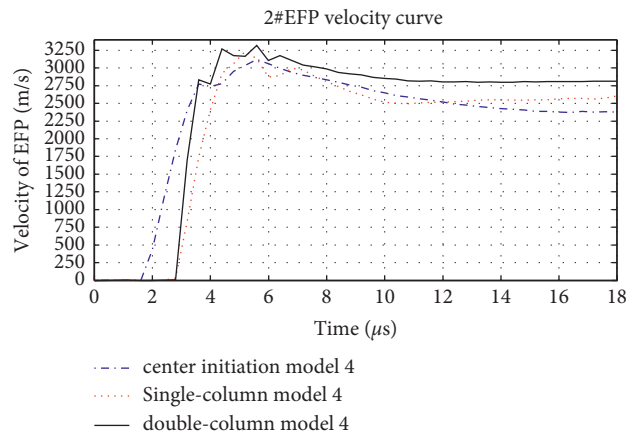
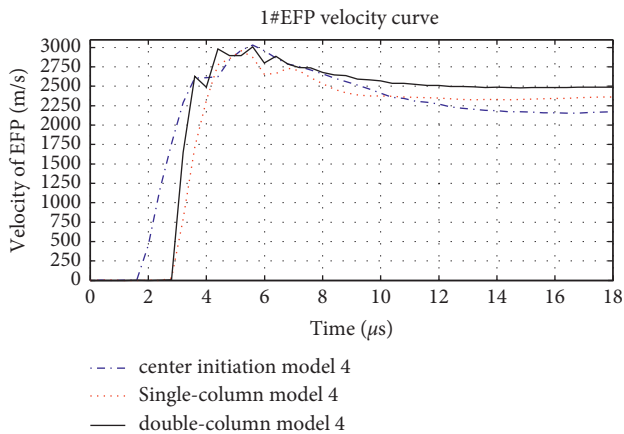


FIGURE 16: Continued.

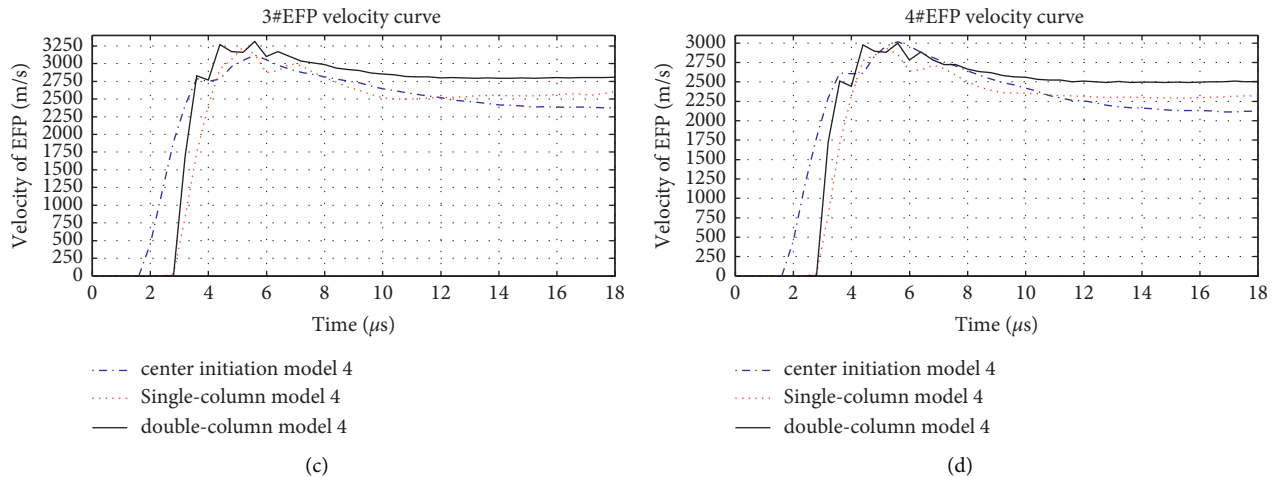


FIGURE 16: The velocity comparison of the fourth group.

column model 4 is 8.4% higher than the velocity of the center initiation model 4. From the above data, it can be seen that the velocity of the double-column model 4 is 5%–7.5% higher than that of the single-column model 4, the velocity of the double-column model 4 is 12%–16% higher than that of the center initiation model 4, and the velocity of the single-column model 4 is 8%–9% higher than that of the center initiation model 4.

## 5. Conclusion

In this study, the circumferential MEFP warhead technology is combined with the directional warhead technology, and three kinds of initiation modes are designed and simulated. The results of numerical simulation show that when MEFP warhead adopts central single-point (multipoint synchronous) initiation, the number of shaped projectiles is the most, and the velocity of the central multipoint synchronous initiation is higher than that of the central single-point initiation; however, compared with the eccentric initiation MEFP warhead, the EFP velocity is lower. Compared with the central initiation, when the MEFP warhead adopts eccentric detonation, the number of formed projectiles is smaller, but the velocity is higher; among them, the MEFP warhead adopts double-column eccentric initiation. The maximum velocity can reach 2814 m/s. Through the comparative analysis of the forming velocity of three types of initiation modes, it can be seen that the velocity of double-column multipoint eccentric synchronous initiation is 2%–9% higher than that of the single-column single-point (multipoint eccentric synchronous) detonation, the velocity of double-column multipoint eccentric synchronous initiation is 10%–17% higher than that of the central single-point (multipoint synchronous) initiation, and the velocity of single-column single-point (multipoint eccentric synchronous) initiation is 5%–17% higher than that of the central single-point (multipoint synchronous) initiation. Different from the directional fragment warhead, the EFP warhead cannot increase the number of EFPs in the directional area, that is to say, the density gain of the kill element. However, it can improve the velocity of local EFP,

that is, the velocity gain of the kill element, so as to improve the penetration ability of EFP to targets and improve the damage efficiency of the MEFP warhead.

## Data Availability

The data that support the findings of this study are available from the corresponding author upon reasonable request.

## Conflicts of Interest

The authors declare that they have no conflicts of interest.

## Acknowledgments

This work was financially supported by the Science and Technology on Electromechanical Dynamic Control Laboratory, China, no. 6142601200408.

## References

- [1] F. Y. Lu, X. Y. Li, and Y. L. Lin, *Structure and Principle of Warhead*, Science Press, Beijing, China, 2009.
- [2] C. X. Zhao, F. Qian, J. G. Xu, H.-A. Cao, C. Ji, and L. Lu, "Effect of liner configuration parameters on formation of integral MEFP," *Chinese Journal of Energetic Materials*, vol. 24, no. 5, pp. 485–490, 2016.
- [3] J. P. Yin and Z. J. Wang, *Ballistics*, Vol. 5, Beijing Institute of Technology Press, Beijing, China, 2005.
- [4] J. Liu, Y. Long, C. Ji, M. Zhong, Y. Liu, and X. Li, "Experimental and numerical study on the dispersion patterns and penetration properties of MEFP with seven arc-cone liners," *Latin American Journal of Solids and Structures*, vol. 14, no. 6, pp. 1064–1084, 2017.
- [5] J. F. Liu, Y. Long, C. Ji, Q. J. Xu, F. Y. Gao, and C. X. Zhao, "Numerical and experimental study on the formation and dispersion patterns of multiple explosively formed penetrators," *Latin American Journal of Solids and Structures*, vol. 14, no. 4, pp. 685–699, 2017.
- [6] R. Fong, W. Ng, B. Rice, and S. Tang, "Multiple explosively formed penetrator (MEFP) warhead technology



- development,” in *Proceedings of the 19th International Symposium of Ballistics*, pp. 7–11, Interlaken, Switzerland, December 2001.
- [7] C. X. Zhao, Y. Long, Y. S. Sui, C. Ji, and X. Zhou, “Influent of initiation methods on formation of integral MEFP warhead parameter,” *Journal of PLA University of Science and Technology (Natural Science Edition)*, vol. 13, no. 5, pp. 559–564, 2012.
- [8] X. Zhou, Y. Long, D. Q. Yu, X. B. Yue, C. Zhang, and W. Xie, “Numerical simulation and effect analysis for radial dispersion of MEFP,” *Acta Armamentarii*, vol. 27, no. 1, pp. 23–26, 2006.
- [9] C. X. Zhao, Y. Long, C. Ji, D. F. Xu, F. Y. Gao, and L. Lu, “Numerical simulation and experimental research on integral multiple explosively formed projectile warhead,” *Acta Armamentarii*, vol. 34, no. 11, pp. 1392–1397, 2013.
- [10] C. X. Zhao, D. Y. Ran, K. Liu et al., “Effect of charge parameters on formation of integral multiple explosively formed projectiles,” *Chinese Journal of Energetic Materials*, vol. 25, no. 11, pp. 882–887, 2017.
- [11] J. P. Yin, Z. H. Yao, and Z. J. Wang, “Influence of liner parameters on the forming of circumferential MEFP,” *Chinese Journal of Explosives and Propellants*, vol. 34, no. 6, pp. 53–57, 2011.
- [12] Z. G. Liang and J. W. Jiang, “A numerical analysis on the forming law of circumferential MEFP journal of projectiles,” *Rockets, Missiles and Guidance*, vol. 35, no. 2, pp. 57–64, 2015.
- [13] Z. G. Liang, B. X. Chen, Y. X. Nan, J. W. Jiang, and L. Ding, “Research on the computing method for the forming velocity of circumferential multiple explosive formed projectiles,” *The Journal of Defense Modeling & Simulation*, vol. 17, pp. 1–12, 2019.
- [14] Z. H. Yuan, Q. H. Chen, and H. B. Li, “Influence of shell on the forming of circumferential MEFP,” *Journal of Defense Modeling and Simulation: Applications, Methodology, Technology*, vol. 18, no. 1, pp. 13–20, 2017.
- [15] C. J. Zheng, Z. G. Chen, J. P. Fu, X. Z. Zhang, W. Z. Wang, and Y. P. Lan, “The structural design of integral MEFP warhead,” *Machine Design and Manufacturing Engineering*, vol. 47, no. 2, pp. 123–127, 2018.
- [16] P. Li, B. H. Yuan, X. Y. Sun, G. Li, and J. Z. Li, “Experimental research on eccentric initiation MEFP warhead,” *Acta Armamentarii*, vol. 38, no. 3, pp. 447–453, 2017.
- [17] W. B. Li, X. M. Wang, W. N. Li, and Y. Zheng, “Feasibility research on the formation of a multimode explosively formed penetrator with single-point initiation,” *Explosion and Shock Waves*, vol. 31, no. 2, pp. 204–209, 2011.
- [18] J. Luo, J. W. Jiang, and B. X. Zhu, “The effect of multile-point initiation on the explosively formed penetrator formation,” *Journal of Projectiles, Rockets, Missiles and Guidance*, vol. 24, no. 2, pp. 27–29, 2004.
- [19] C. X. Zhao, Y. Long, C. Ji, Y. C. Li, Q. M. Xie, and L. Lu, “Distribution law of pressure on liner surface under multi-point initiation,” *Chinese Journal of High Pressure Physics*, vol. 27, no. 1, pp. 83–89, 2013.
- [20] J. Q. Liu, W. B. Gu, H. M. Xu, M. Lu, and S. Z. Wu, “Effects of multi-point initiation charge configuration parameters on EFP with fins formation,” *Chinese Journal of Energetic Materials*, vol. 22, no. 5, pp. 594–599, 2014.
- [21] R. Li, W. B. Li, X. M. Wang, and W. B. Li, “Effects of Three-point initiation control parameters on formation of explosively- formed projectiles with fins,” *Explosion and Shock Waves*, vol. 38, no. 3, pp. 501–508, 2018.
- [22] G. Ma, G. He, Y. Liu, and Y. Guo, “Study of the forming characteristics of small-caliber ammunition with circumferential MEFP,” *Materials*, vol. 13, no. 4, pp. 1–24, 2020.